

Time-dependent Microcracking Detected in a Rubber-toughened Carbon-epoxy Composite by the Modal Acoustic Emission Method

R. T. BOCCHIERI*

Applied Research Associates, Inc.

2672 Bayshore Parkway

Suite 1035, Mountain View, CA 94043, USA

R. A. SCHAPERY

The University of Texas at Austin

Austin, TX 78712, USA

M. R. GORMAN

Digital Wave Corporation

11234-A East Caley Avenue

Englewood, CO 80111, USA

ABSTRACT: A method of modal acoustic emission monitoring and waveform analysis is developed as a means for tracking two of the primary damage mechanisms in unidirectional composite lamina, matrix-cracking and fiber-matrix debonding. Unidirectional 30, 45 and 90° coupons of a rubber-toughened carbon-epoxy are monitored in this way for various loading histories. A method of comparing waveforms from different samples is proposed in order to establish the similarity of microcracking regardless of fiber direction. Histograms of waveform energy are used as a measure of average arrested crack length versus stress level. Larger faster cracks will emit more energy. Finally, an interpretation of the AE data is given based on an initial population of existing flaws where a cumulative distribution function (CDF) of microcracking is defined and used to study effects of stress history.

KEY WORDS: microcracking, composite material, modal acoustic emission, damage, viscoelasticity, rubber-toughened.

*Author to whom correspondence should be addressed. E-mail: rbocchieri@ara.com

INTRODUCTION

MANY POLYMERIC COMPOSITE materials experience ply-level microstructural damage at loads far below their failure stress [1]. At the ply-level, damage refers to microstructural changes such as matrix cracking and fiber–matrix debonding distributed throughout the material. Such microcracking can have a significant softening effect in the off-axis fiber directions. Although this softening may not have a significant impact on the overall stiffness of a structure, knowledge of the ply level stresses is needed to make predictions of more serious forms of damage such as transverse cracking, delamination and finally fiber failure. Indeed, these larger scale damage forms, prior to catastrophic failure, may themselves be ‘design-driving’ failure modes depending on the application and play a critical role in material durability.

As the polymer matrix is a viscoelastic material, cracking of the matrix between the fibers and at the fiber–matrix interface will be time or rate-dependent. Large scale cracking, such as transverse cracking, has also been seen to be time-dependent for some materials [2]. Depending on the material, this time-dependence may be weak at room operating conditions, but can increase significantly at elevated temperature. The rubber-toughened composite studied herein displayed significant time-dependent microcracking even at room temperature starting at less than half of the ply failure stress.

In an independent microscopy study by Wood and Bradely [3] on the same carbon-epoxy in this study, it was found that matrix cracking and fiber–matrix debonding were indeed the dominant damage mechanisms viewed in this material. They developed a special sample geometry for viewing the material under load in an environmental SEM and found a variety of initial flaws in the material prior to loading, including voids, cracks around voids and fiber–matrix debonds. During loading, the damage events include formation of new debonds, opening of debonds, cracks at the edges of voids connecting to debonds and the coalescing of debonds. Damage first initiates at the boundaries of resin rich regions and later initiates in other regions at higher stress. Other possible damage not observed by Wood and Bradely is the cavitation of rubber particles and the subsequent shear yielding around these particles.

Much of damage mechanics uses continuum theories which implement damage variables to relate the size, shape and orientation and density of cracks with the global response (e.g. [4,5]). Schapery [6,7] developed a constitutive theory for elastic media with growing damage based on irreversible thermodynamics, where internal state variables were used to describe the effect of microstructural changes. Schapery [8] and Schapery and Sicking [9] applied the model to a carbon-epoxy composite. One simplifying feature of these theories is that all permanent softening is due to the growth of this damage. The damage state is directly tied to the amount of softening observed in the stress–strain behavior. When the softening effects of damage are coupled with viscoelasticity and/or viscoplasticity, softening occurs due to the inherent viscoelastic behavior of the undamaged material, the growth of damage, and time-dependent opening or sliding of the crack faces that have formed. Just determining which softening mechanism is responsible for the observed behavior becomes more complicated. The rate of damage growth itself may depend on the entire loading history in a fashion which needs to be experimentally determined.

When a material contains all possible softening mechanisms (i.e., nonlinear viscoelasticity, viscoplasticity and damage) there is no apparent way to isolate the effect of damage and its growth from the other softening mechanisms based solely on

stress–strain data because established mathematical models for mechanical behavior are too limited at this time. In this case, direct damage monitoring is needed. Tracking the density of transverse cracking (large scale cracking, typically of an entire ply), for example, has been shown to be a good damage parameter for predicting softening in cross-ply laminates under tensile load (e.g. [1]). Density of such cracking has been measured by various means, including X-ray radiography, polar backscatter scans, edge-replication and acoustic emission monitoring. In the present study, the scale of individual cracks is smaller by an order of magnitude and distributed three-dimensionally throughout the material. Any form of visual inspection to ‘count microcracks’ is simply an intractable situation. A real-time, efficient method for tracking this type of damage is needed. Monitoring their acoustic emissions may be the only practical means. The major focus of this study is to develop a means for tracking and analyzing microstructural damage progression using the modal acoustic emission method.

A large number of acoustic emission studies (frequently using older AE technologies) involve attempts to differentiate forms of damage occurring concurrently in a laminate (e.g. [10–13]). For example, in any but a unidirectional material, fiber breaking, microcracking, fiber–matrix debond, transverse cracking (or ply-failure), and delamination may all occur during a test. Each mechanism has its own effect on the degradation of the material and each, in principle, could have a particular acoustic (ultrasonic) signature. As the focus of this study is on ply-level matrix-dominated behavior, we are primarily interested in AE testing performed on off-axis unidirectional laminates, that is with all fibers at the same nonzero angle relative to loading, which eliminates many of these damage mechanisms from occurring.

A relatively small amount of acoustic emission testing has been published on unidirectional laminates of polymeric composites. Even with testing in the fiber direction, multiple damage mechanisms can occur. These studies cover several methods to discern matrix-cracking, debonding and fiber breakage and fiber pull-out from one another with mixed success (e.g. [14–18]). A few studies have been published for loading in the off-axis directions ([19,20]). However, in one case [20] a single sensor was used so that the source of the events is unknown, making any meaningful interpretation of the data difficult if not impossible. However, Okoroafor [20] did demonstrate the utility of acoustic emission monitoring to evaluate the effect of different sizings on fiber–matrix adhesion. He established definite trends in the AE data as the adhesion was reduced.

At this time, a one-to-one correspondence between an observed micro-fracture event and its detected acoustic wave is not possible in standard tensile coupons due to the very small scale of cracking. Consequently, several steps are taken here to methodically eliminate other acoustic sources so that only the fracture mechanisms of matrix cracking and fiber–matrix debond are considered. In particular, a novel method of testing off-axis samples is introduced where two broadband sensors are used to discern events occurring in the uniformly stressed portion of an off-axis sample from those occurring elsewhere. Also, testing was performed using a relatively new method of acoustic emission monitoring, called Modal AE, where waveforms are acquired digitally and waveform analysis is performed based on principles of elastic wave propagation.

Unidirectional material in its as-manufactured state contains a statistical distribution of small flaws or cracks that serve as initiation sites for microcrack growth. This distribution should be essentially common to all samples manufactured in a similar fashion. Therefore, a major goal was to find a measure of this distribution of flaws and to determine experimentally the effect of loading history on their growth. Experiments were run on 90°

and other off-axis unidirectional samples using various loading histories so that the time or rate dependence of cracking could be studied and the microcracking for different fiber angles compared.

First, waveforms measured from two broadband sensors on each sample type are reviewed in this paper. Next, a new method, suggested by one of the authors (M.G.), for separating the detected plate waves into their extensional and flexural modes is also discussed. This method, along with two sensors used for location, is used to compare fracture events in different sample types so that differences in attenuation with fiber direction and distance can be eliminated. Next, a histogram of event energy versus load level is used to study the effect of global stress level as a measure of arrested crack length. This study also indicates whether the 'detectability' of a given flaw, when it grows dynamically, changes during the test, thereby affecting the perceived distribution of flaws. Changes in material acoustical properties as the material is loaded are also considered. Finally, data collected from 90, 45 and 30° off-axis samples loaded with various histories are used to construct a cumulative distribution function of the microcracking detected.

EXPERIMENTAL ARRANGEMENTS

The material studied was comprised of AS4C carbon fibers with a rubber-toughened epoxy resin E719LT produced by BP Chemicals. Details on its manufacture can be found in [21]. The composite was produced by R-cubed composites with a maximum cure temperature of 121°C (T_g is approximately 120–125°C) and a fiber volume fraction of approximately 57%. The rubber content is approximately 5% by volume. Unidirectional 6-ply plates were cut into 90, 45, and 30° off-axis samples with a diamond grinding wheel to minimize edge damage. This selection of samples affords three combinations of the primary ply stresses so that the effect of shear to transverse stress ratio can be examined. All constant stress rate testing was performed on an Instron screw-driven load frame 4505 with Instron 4500 controller at room temperature and humidity conditions (moisture absorption of the desiccated samples for short-term testing is negligible). All hardware and software used for acoustic emission data acquisition and analysis, as shown in Figure 1, were provided by Digital Wave Corporation.

Isolation of the AE Sources

In all AE testing it is best to have a one-to-one correspondence between a visually observed fracture event and its detected acoustic wave for the purpose of calibration. In this way, there is no question about the emission source. This has been done with good accuracy for large scale cracking, such as transverse cracking in cross-ply laminates, where the entire ply fails ([22,23]). In this paper, the acoustic signals were used to locate the position of a given crack by modal analysis of the waveform and subsequent wavespeed calculation. These locations correlated well with those cracks that could be observed by polar backscatter scans, thus serving to check the modal analysis method. Our goal, however, is to detect much smaller events that are below the scale where they can be observed by polar backscatter scans, X-radiography or edge-replicate techniques.

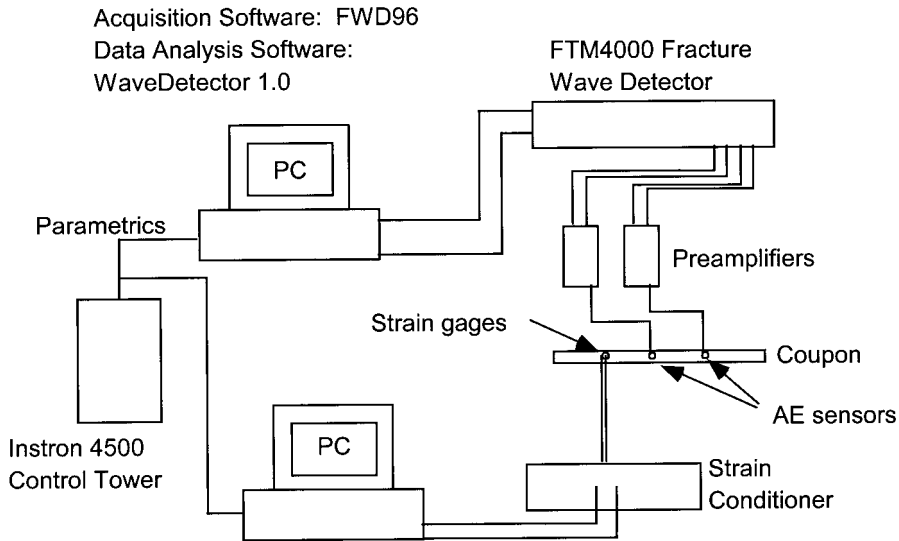


Figure 1. Hardware and software configurations used for acoustic emission and stress-strain data acquisition.

Several steps were taken to ensure that only the events caused by the damage mechanisms reported by Wood and Bradely [3] were accepted for analysis. First, as will be further discussed, events were accepted only from the free-length of the material by locating the event source using two sensors. Locating events, found to be evenly distributed along the free-length, eliminates the possibility of a singular flaw growing intermittently causing the AE signals. Second, by using simple unidirectional samples, we have limited the number of types of damage to matrix cracking, fiber-matrix debonding, rubber-particle cavitation and fiber breakage. By testing in the 90° and off-axis directions, the possibility of significant fiber breakage is eliminated. A neat sample of the rubber-toughened matrix was also loaded to failure. The few events detected were found to correlate with a few cracks which developed prior to failure [24]. Thus, there is no indication that rubber particle cavitation is detectable with the AE sensors used.

Frictional sliding may also produce acoustic emissions [25] and will occur repeatedly whenever the material is loaded and unloaded. As will be shown in the results, practically all events captured occur only during the loading portions, indicating that frictional sliding does not produce acoustic signals in these samples. A final possibility is that edge-cracking provides the predominant amount of signals from the free-length. However, as will also be shown in the results, the onset of nonlinearity in the rubber-toughened material coincided with the onset of significant acoustic emissions, indicating that these phenomena are related. If only edge cracking caused significant material softening, there would be a sample width effect on the stress-strain nonlinearity, this effect did not exist [21]. By deduction, we are therefore left with distributed matrix-cracking and fiber-matrix debonding as the primary mechanisms causing the acoustic signals. It is interesting to note that microcracking was not detected with the same testing apparatus in two untoughened composites, T1000/8852 (carbon-epoxy) and S2/8852 (glass-epoxy), when tested in various off-axis directions. These materials also displayed little nonlinearity in their stress-strain response prior to failure.

Anticipated Waveforms and Detection

Two types of detectable damage are expected in the unidirectional material when loaded off-axis to the fibers, matrix cracking and fiber–matrix debonding. If a sufficiently thin sample is used, it is anticipated that both damage forms will create a waveform that is a combination of extensional and flexural plate waves. Gorman and Ziola [22] found this to be the case for transverse matrix cracking in cross-ply laminates.

Samples were chosen to ensure that extensional and flexural plate waves were detected from the anticipated damage modes. For this to hold true, sample thickness was chosen on the order or less than the wavelength of the emitted waves [26]. This can be checked by first calculating the speed of the extensional mode, which is independent of frequency, and is given by [22]

$$C_e = \sqrt{\frac{A_{xx}}{\rho h}} \quad (1)$$

where A_{xx} is the first component of the laminate force–strain stiffness matrix, as given by lamination theory (e.g. [27]). Density is ρ and h is laminate thickness. Speed of the flexural mode is given by

$$C_f = \left(\frac{D_{xx}}{\rho h}\right)^{1/4} \sqrt{\omega} \quad (2)$$

where D_{xx} is the first component of the moment–strain stiffness matrix and ω is the frequency.

It is expected that microcracking and debonding will create a predominantly extensional wave that always travels faster than the flexural mode and has minimal dispersion below 1 MHz. The extensional mode was therefore used for location finding and also used for the calculation of wavelength. As will be shown in the results, a predominant amount of waveform energy detected in this material has frequencies from approximately 100 to 400 kHz. Extensional wavespeed was calculated to be approximately 2450 m/s corresponding to a wavelength of 6.1 mm (for 400 kHz). Thin 6-ply coupons, 1.65 mm thick, were used for all modal acoustic emission (MAE) testing to ensure that plate waves were dominant.

AE Testing of Unidirectional Specimens

Two types of broadband sensors were used for MAE monitoring; the B1025 sensor, which offers a wide range of sensitivity up to 1.5 MHz and the B225 sensor, with approximately four times the sensitivity of the B1025 up to 500 kHz. Most testing of the 90° samples was performed with the B1025 sensor, but the B225 was needed to detect microcracking in the off-axis samples. These sensors were attached to a sample with electrical tape, as shown in Figure 2, after applying high vacuum grease to the sensor faces. A free length of nominally 5 cm was found to provide good sensitivity to small events without sacrificing location accuracy. Strain gages were placed outside the free length as

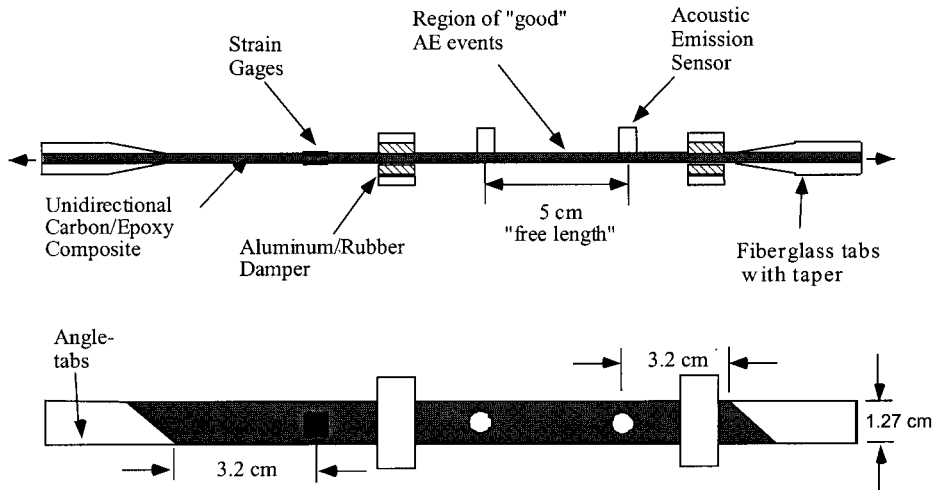


Figure 2. Unidirectional coupon shown with strain gages, acoustic emission sensors and dampers.

the strain gage bond system gave off acoustic events at many stress levels. Aluminum/rubber dampers were lightly clamped onto the sample to reduce noise coming from the gripped/tabbed regions. A simple experiment using lead-breaks indicates that these dampers reduce the maximum amplitude of a lead-break, located within 1 cm of a sensor, by approximately 40%.

Angled tabs ([21,28,29]) were used to ensure a uniform stress region of adequate size to detect AE events, which we will call 'good events', and to take strain readings. The effect of changes in wavespeed with fiber direction must also be considered for off-axis samples. The relative arrival time of an extensional acoustic wave (the difference in arrival times of the acoustic wave at each sensor) emanating from a crack at the top edge, centerline, and bottom was calculated for a sensor spacing of 4.7 cm and plotted in Figure 3 for a 30° off-axis sample. To validate sensor spacing and these calculations, lead breaks were performed at several locations between and outside the sensors prior to running each test. If all events were assumed to originate from the centerline of the sample and linearly located along the length, events from outside the sensors may be accepted. However, these events may be originating from nonuniform stress regions or the strain gages. This complexity can be managed by adopting an acceptance criterion of 12 μ s, for example, as illustrated in Figure 3. An area represented by the shaded region indicates the volume of material from which events are then accepted. A skewed volume has no consequence as long as it is under uniform stress.

RESULTS

Stress–Strain Behavior

Shown in Figures 4 and 5 are the axial stress–strain response of 90 and 30° off-axis samples tested at various loading rates. The nonlinearity and time-dependence of this material is evident from both samples, but definitely stronger with the presence of shear stress in the 30° samples. The onset of microcracking, as detected by the AE sensors, is

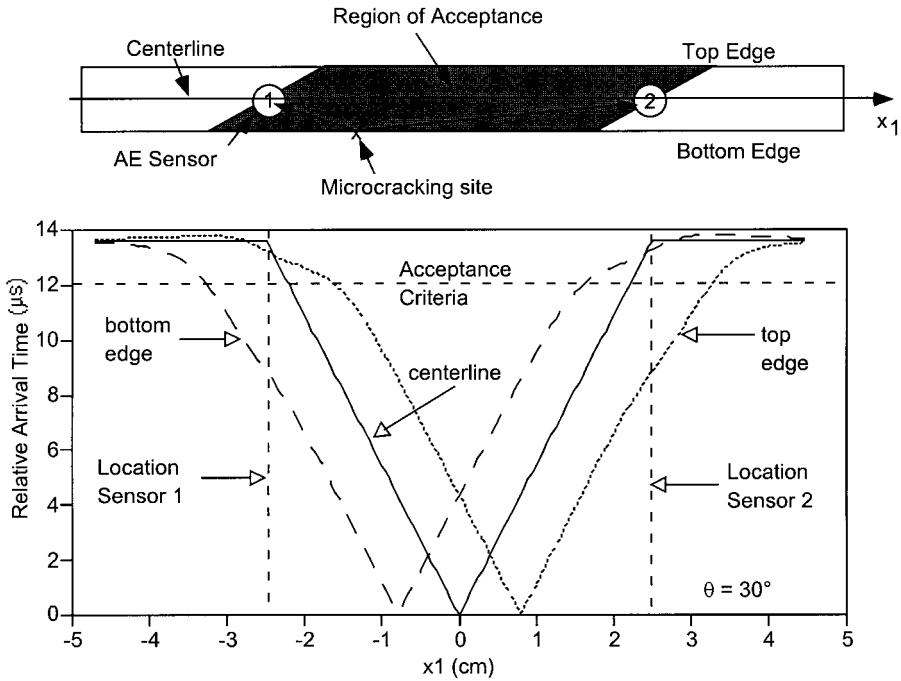


Figure 3. Relative arrival times for events occurring at the bottom edge, center, and top edge of a 30° off-axis sample.

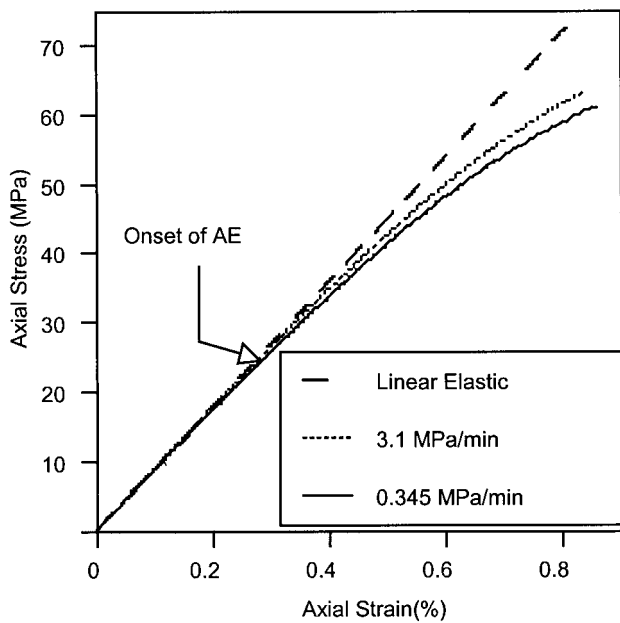


Figure 4. Axial stress–strain response of 90° unidirectional samples tested at two different load rates.

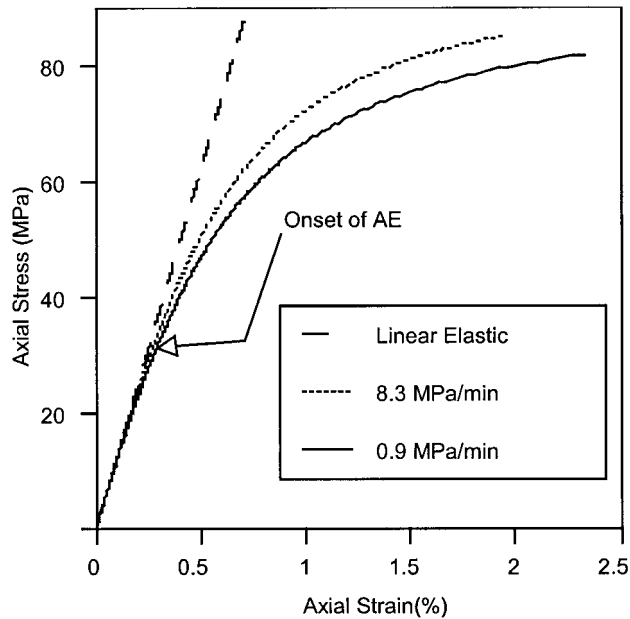


Figure 5. Axial stress–strain response of 45° off-axis samples tested at two different load rates.

indicated in each figure. Isolation of the various mechanisms causing this nonlinearity and rate-dependence, including damage growth, can be found in ([24,30]).

Location of AE Events

An initial threshold-crossing criterion, slightly greater than the noise amplitude, was used to calculate arrival time at the two sensors. In this way, the nondispersive extensional wave is used for location finding. Thousands of events were typically detected during a test so it was not practical to use more accurate location techniques such as manual phase matching. As we are only concerned with whether an event came from the free length, and not finding its exact location, this technique was sufficient and expedient. To be conservative, any events found within 5 mm of a sensor were not accepted. If an event was detected on only one sensor it was also discarded. After all events were filtered by the aforementioned techniques and reduced to a more manageable number, the events were visually inspected for any that may have slipped through this process.

Significant cracking, evenly distributed along the length of 90° and off-axis samples, was detected with the AE sensors. A typical histogram of locations in the free length of a 90° sample is shown in Figure 6, indicating that cracking is distributed along the length, not isolated to specific regions of the material, as desired.

Cumulative Events Versus Load Level

CONSTANT STRESS RATE EXPERIMENTS

Cumulative AE events detected in 90° samples are plotted versus axial stress in Figure 7. There is no pattern with loading rate. Apparently, there is significant scatter

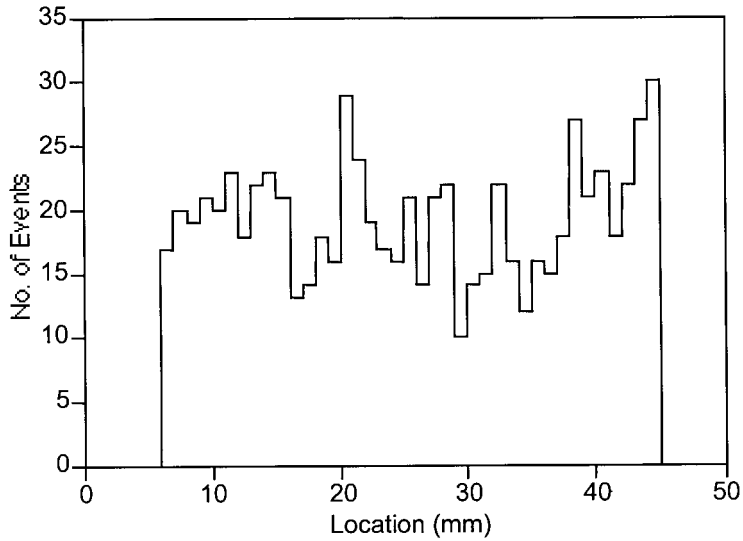


Figure 6. Location histogram of microcracking in the free length of a 90° sample.

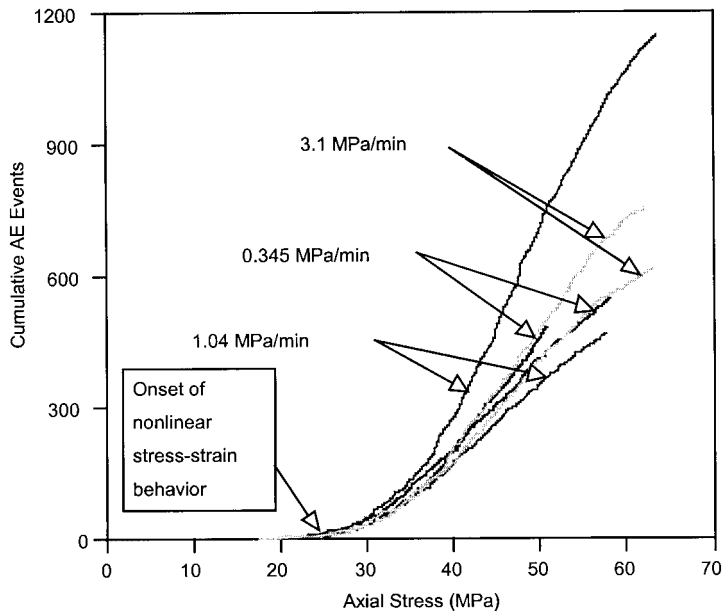


Figure 7. Cumulative AE events detected in 90° samples vs. axial stress for three loading rates. All testing was performed with B1025 sensors.

between samples in terms of the number of detectable events. Up to twice the number of events were detected in separate samples tested at equal rates. Emissions detected from 45° and 30° off-axis samples are shown in Figures 8 and 9. Note that in Figure 9 when the B1025 sensors were used, the less sensitive sensors, far fewer events were detected. There is a large swing in event count at high stress when using

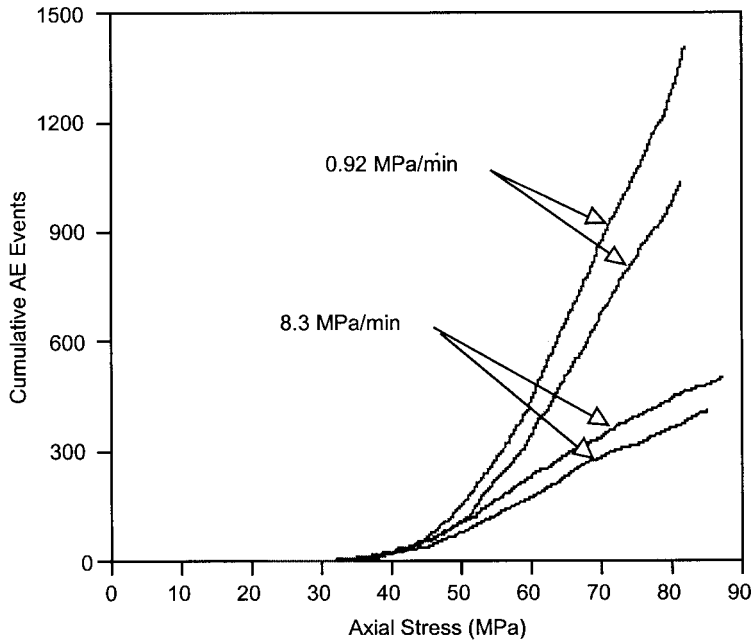


Figure 8. Cumulative AE events detected in 45° off-axis samples vs. axial stress for two loading rates. All testing was performed with B225 sensors.

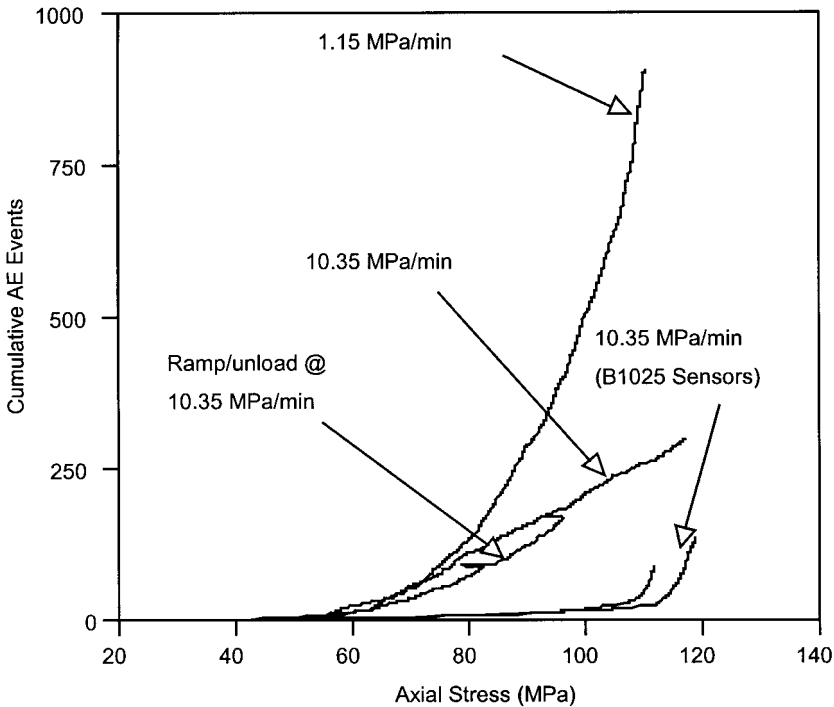


Figure 9. Cumulative AE events detected in 30° off-axis samples vs. axial stress for two loading rates. All testing was performed with B225 sensors except for the two specified.

these sensors. Since this upswing was not seen when using the more sensitive sensors, we may conclude that the events at high stress are of greater magnitude and a study of event magnitude is needed.

LOAD/UNLOAD EXPERIMENTS

Loading/unloading cycles were performed on 90 and 30° off-axis samples to see if the detected events are indicative of friction. As shown in Figures 10 and 11, the detected events do not display a pattern typical of friction effects. Few events are detected during unloading and the ones that are detected occur predominantly close to the highest stress attained. Upon reloading, few are detected until the previous stress is approached.

RAMP/HOLD EXPERIMENT

In order to exaggerate time-dependent cracking in the 90° samples, a ramp hold test was performed with hold periods of 20 h. The loading history and strain responses are shown in Figure 12. Figures 13 and 14 show cumulative events versus time under load and stress, respectively. Significant time-dependent damage is evident from the large accumulation of

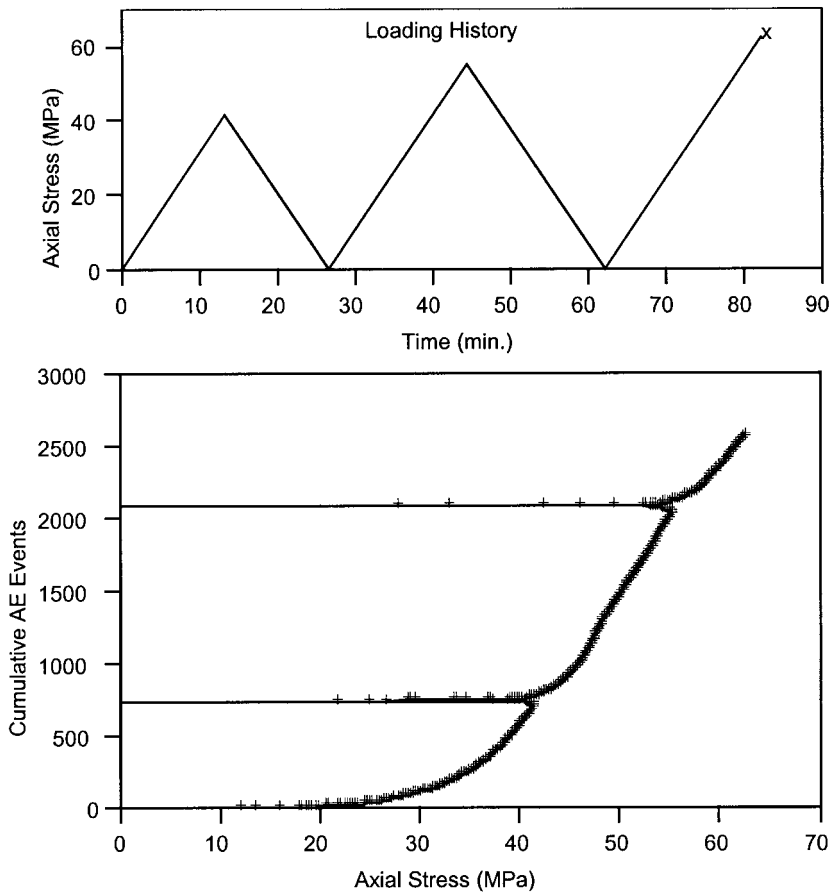


Figure 10. Cumulative events detected in a 90° unidirectional sample during loading/unloading and reloading cycles. The loading history is shown in the top figure.

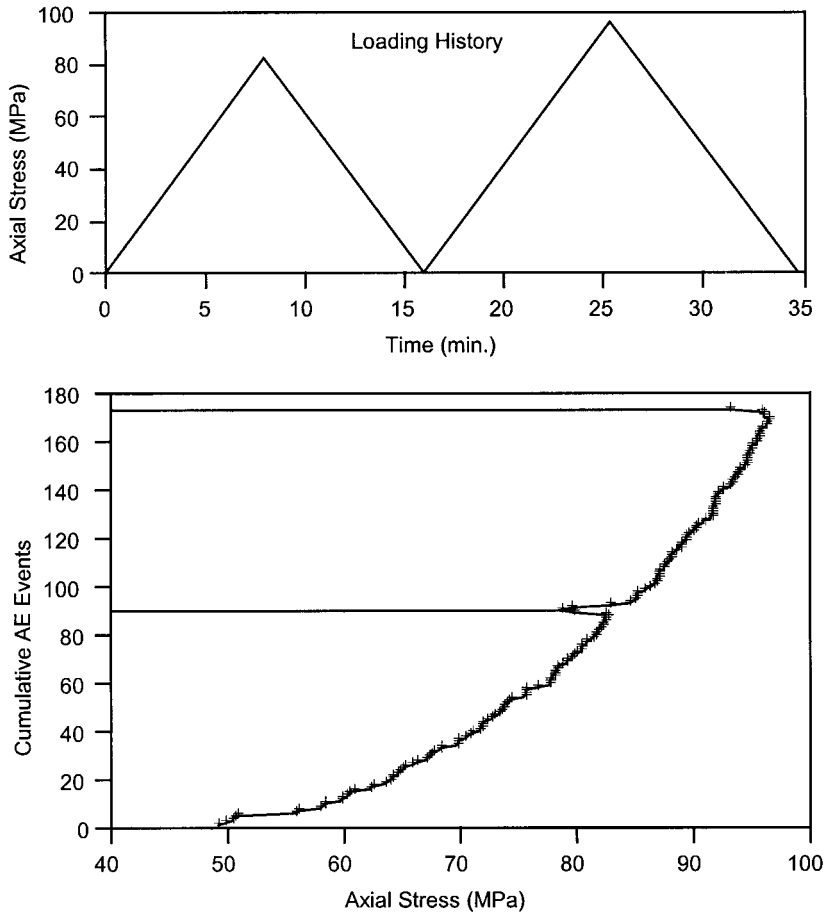


Figure 11. Cumulative events detected in a 30° off-axis sample during loading/unloading and reloading cycles. The loading history is shown in the top figure.

events during the hold periods. Of even greater interest is the behavior seen during the second and third ramp periods shown in Figure 14. During the second load-ramp, damage does not begin to accumulate until the stress was increased by about 6 MPa. During the third ramp, an increase of about 3 MPa is needed for additional damage. Thus, no additional microcracking occurs until the load had increased significantly above the holding stress. This may indicate that microstructural stress relaxation has occurred; the increasing global stress needs to first overcome the internal stress relaxation before more damage growth is induced.

Waveform Analysis

WAVEFORMS DETECTED AT LOCATION SENSORS

A range of waveforms was detected in the rubber-toughened composite by the location sensors. Events varied from those barely detectable with the most sensitive system settings, just above the noise range, to those off-scale. For a given stress level, this can be attributed

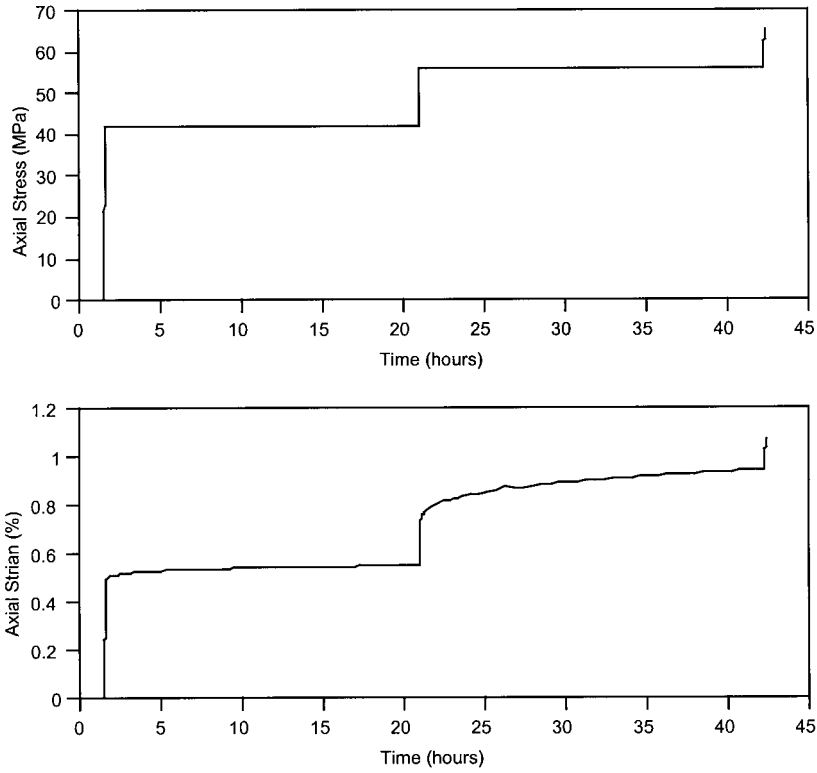


Figure 12. Loading history and strain response from ramp/hold testing.

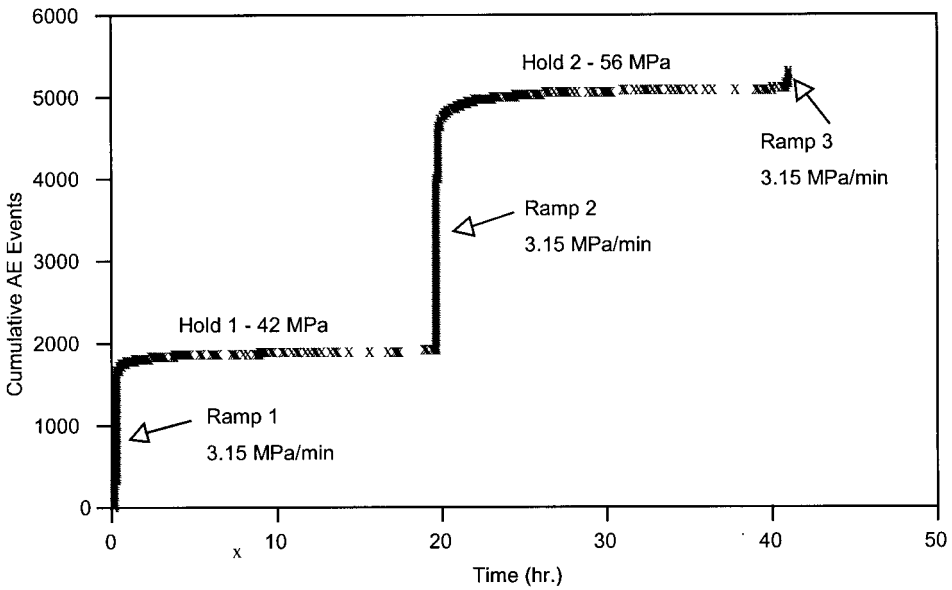


Figure 13. Cumulative AE events vs. time detected during ramp/hold testing of a 90° sample. Testing was performed with B225 sensors.

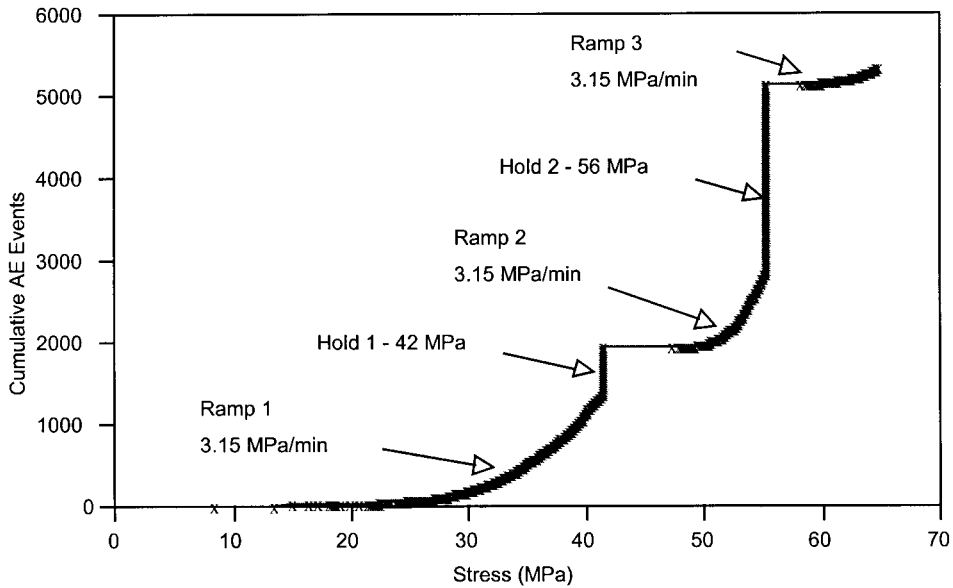


Figure 14. Cumulative AE events vs. stress detected during ramp/hold testing of a 90° sample. Testing was performed with B225 sensors.

to variations in the amount of strain energy released (depending, for example, on initial and arrested crack size), and differences in distance and direction of travel to the sensors. Large attenuation of the higher frequencies was observed even for the short sensor spacing used.

Frequency analysis was performed by first windowing the waveform to remove some of the background noise and wave reflections and then taking the FFT. A 30 μs window was used for events detected from 90° samples and 50 μs for the off-axis samples. Figures 15 and 16 show some typical waveforms detected in 90 and 30° off-axis samples. Windowing is shown with the dotted lines. Notice that the time-scales in these two figures are different. The primary frequency content from all samples tested lay between 100 and 400 kHz. Comparison of events between specimen types cannot be made using the location sensors due to differences in attenuation with fiber angle. A special sensor setup was used for this purpose.

EXTENSIONAL AND FLEXURAL WAVEFORMS

Comparison of microcracking waveforms from different sample types was performed by using the sensor setup shown in Figure 17. Two B225 sensors supply the location of a given event as done in previous testing. The adjacent B1025 sensors were used to evaluate events occurring directly beneath them. In this way, differences in attenuation with direction and distance are eliminated. By suggestion of one of the authors (M.G.), they were placed on opposite sides of the sample so that the extensional and flexural components of the waveform could be discriminated. An extensional waveform is symmetric, with equal displacement on the top and bottom of the sample. A flexural waveform is asymmetric. By adding and subtracting the signals from both sensors, the extensional and flexural components may be extracted. Testing of this nature was performed on both 90 and 30° off-axis samples.

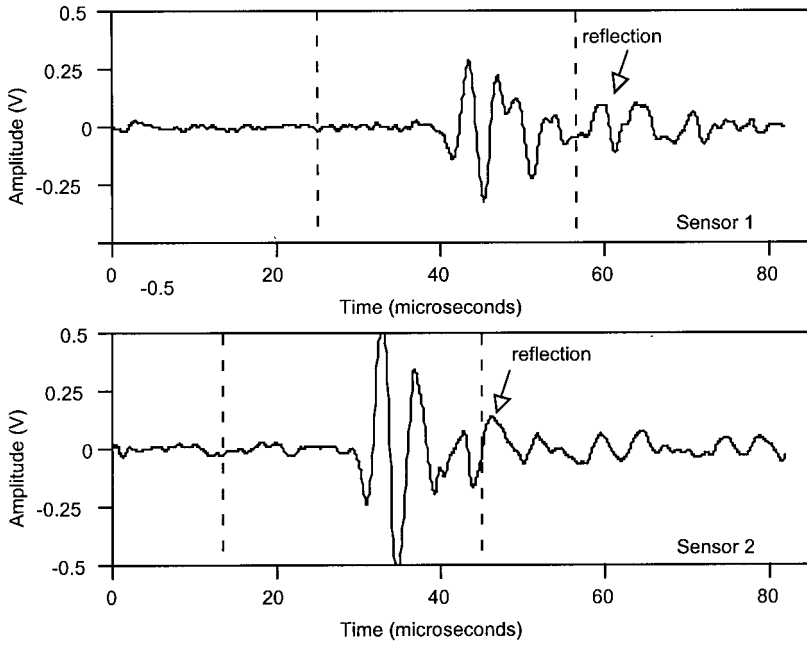


Figure 15. Typical large event detected from a 90° unidirectional sample where microcracking occurred close to sensor 2. The dotted lines indicate the windowing used for waveform analysis. B225 sensors were used ($1\text{ V} = 50\text{ db}$).

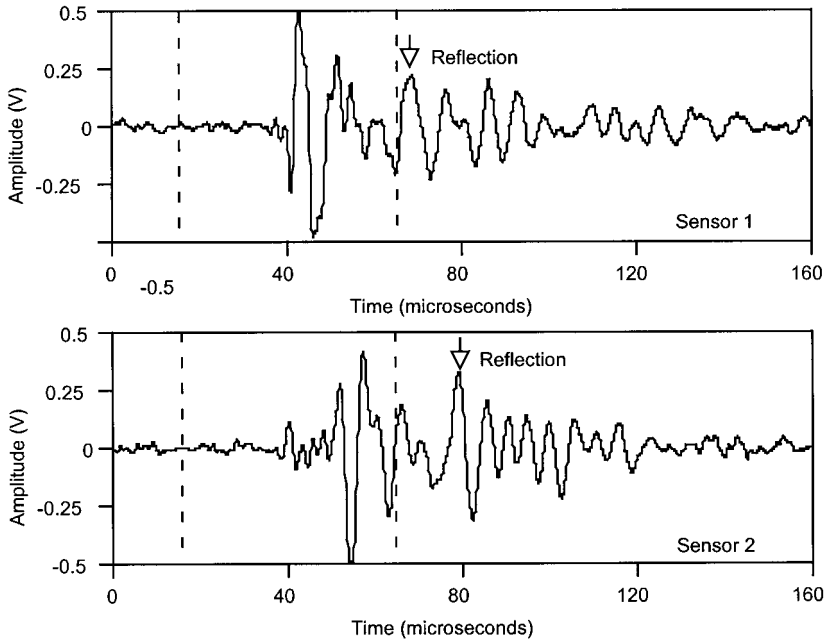


Figure 16. Typical large event detected from a 30° unidirectional sample using B225 sensors ($1\text{ V} = 50\text{ db}$). The dotted lines indicate the windowing used for waveform analysis.

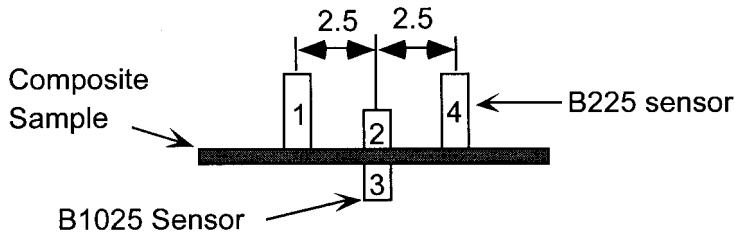


Figure 17. Four sensor setup. Two B225 sensors (1 and 4) are used for location. The B1025 sensors (2 and 3) are used to evaluate waveforms. Units in cm.

Figures 18 and 19 are two examples of waveforms detected in 90 and 30° off-axis samples, using the same windowing as previously mentioned. Variation from event to event makes a comparison of waveforms in both samples difficult. However, there are some similarities. Signal duration of the extensional mode is approximately 5 μ s. The extensional mode is also of greater magnitude than the flexural mode and has similar shape in both samples. Both modes display frequencies covering the entire range of the broadband sensors used. Based on these observations, there is no evidence of a significant difference between the microcracking in 90 and 30° off-axis samples. It may be that any differences do not display different acoustic signatures, or that a large number of events needs to be observed for those differences to become evident. Based on the evidence at hand, events from both samples will be analyzed identically.

Waveform Energy

Distributed microcracking in the material emits a variety of acoustic waves depending on the size of the crack and the local fracture energy of the material that fails. The detected waveform is also affected by the distance of the sensor and direction of travel to that sensor. The energy of a waveform (i.e., the time-integrated squared amplitude) provides a measure of the fracture energy and how much material failed; larger, faster cracks create larger acoustic waves. There was a large variation of this energy from event to event. We are concerned, however, with the 'average' microcracking which is distributed throughout the material. A histogram of event energy versus stress level, which provides an average energy of the microcracking over each stress segment, can therefore provide some insight into how the nature of the microcracking changes as the load and time under load increases. In this way, all variables that affect signal energy (crack size, fracture energy, distance and direction to sensors) is averaged. Event energy was calculated from the signals received by both of the AE sensors using the 'energy' feature of the AE software. Waveforms were windowed, as described in the previous section, so that the effect of background noise and reflections were minimized in the energy calculation. These energies were then averaged over all the events detected for every 2 MPa of loading, as shown in Figure 20 for 90° samples tested with various rates.

The average energy emitted showed no increasing or decreasing trend during loading from first microcracking to failure. This observation has some interesting possible ramifications. First, the average arrested crack length, interpreted here as the amount of crack growth, is not a function of stress level. Here we define the arrested crack length as the initial length subtracted from the final length. Assuming that the energy released is

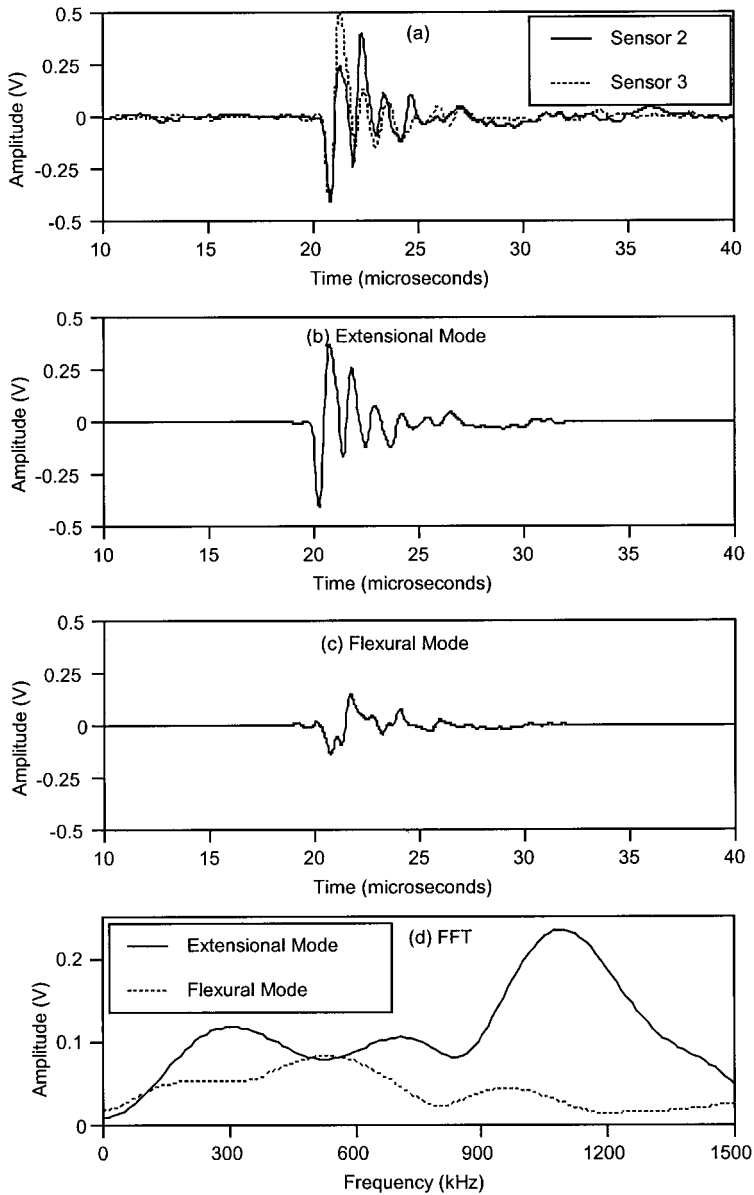


Figure 18. (a) Waveforms detected directly beneath sensors 2 and 3 in a 90° sample; (b) Extensional; (c) Flexural components of the waveform in (a); (d) FFT of the extensional and flexural components. ($1\text{ V} = 47\text{ dB}$).

dominated by arrested crack length, microcracks which initiate at low stress propagate the same average distance as those that initiate at high stress. Second, if cracking occurs both in the matrix and at the fiber–matrix interface and their fracture energies are different, the same portion of cracks initiate in each up until failure. But, there could be competing effects. Regardless, the ‘detectability’ of individual microcracks does not change throughout the test. If the average arrested crack length did increase, and therefore the subsequent event energy, they would be more detectable.

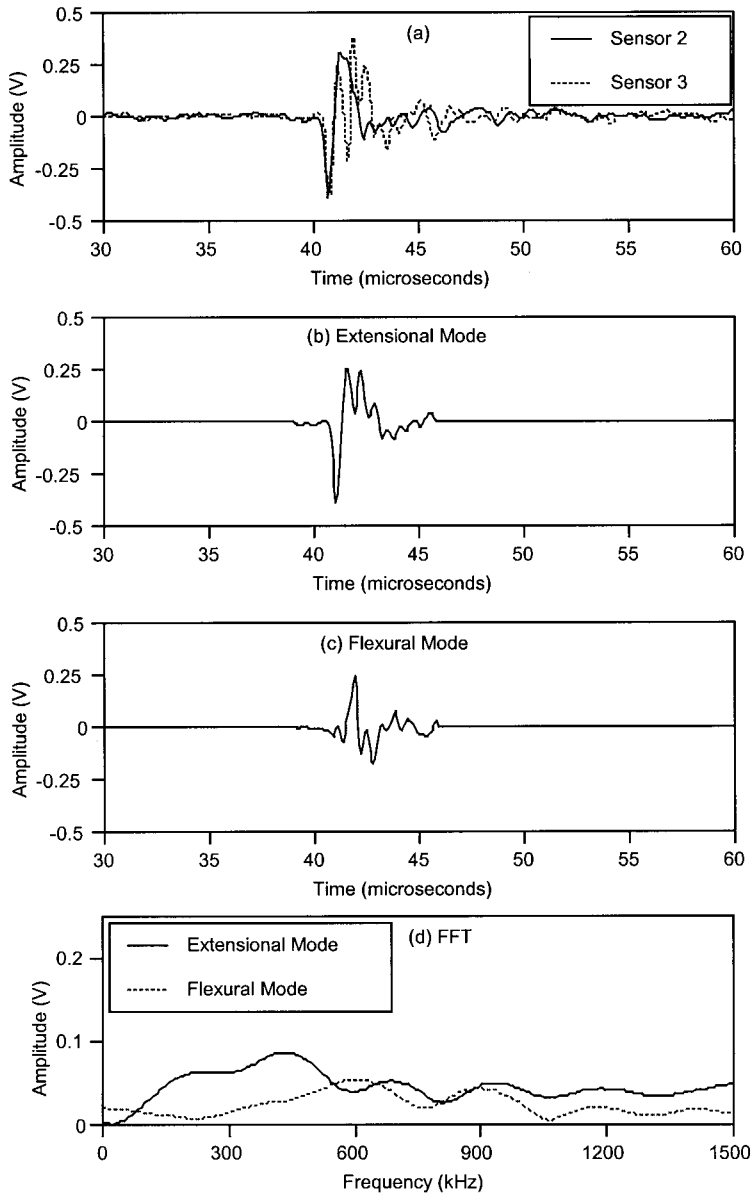


Figure 19. (a) Waveforms detected directly beneath sensors 2 and 3 in a 30° off-axis sample; (b) Extensional; (c) Flexural components of the waveform in (a); (d) FFT of the extensional and flexural components. ($1\text{ V}=47\text{ dB}$).

The existence of shear stress in the matrix of the 30° and 45° off-axis samples does have an impact on the average arrested crack length, however, as shown in Figures 21 and 22. Results from both off-axis samples show an upswing in average event energy at high stress. Using a smaller interval in these histograms, it was found that this upswing in event-energy occurred just prior to failure in the 45° off-axis samples, as shown in Figure 23. These large-energy events account for only 15% of those detected and have

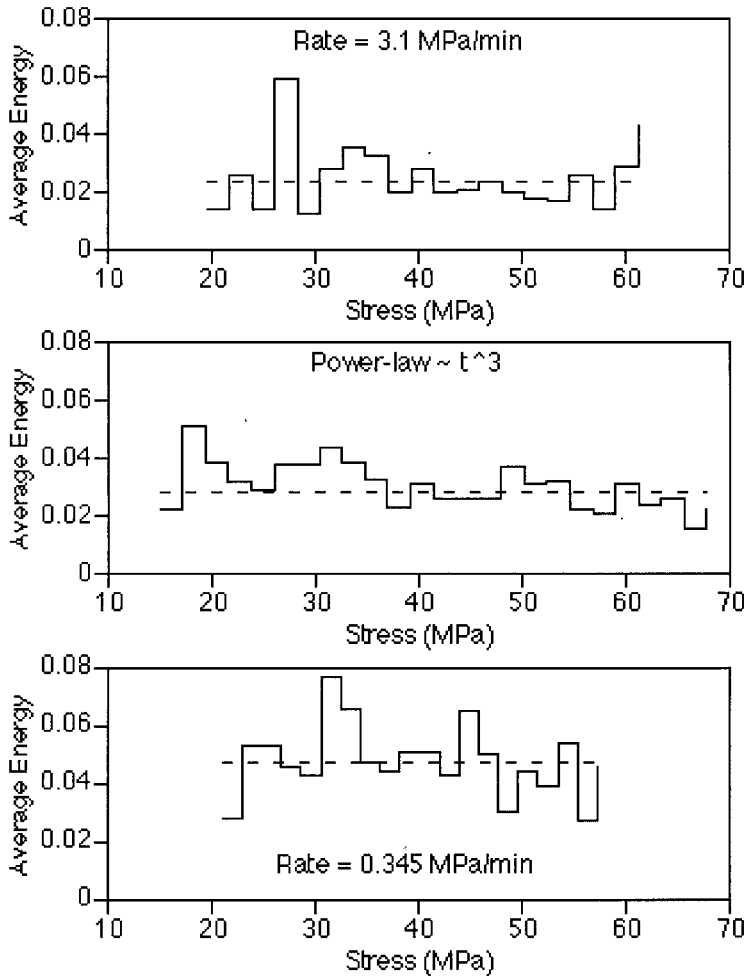


Figure 20. Average event energy detected in 90° unidirectional samples for three loading histories. The mean energy of all events is shown by the dotted line.

little effect on subsequent analysis. When the proportion of shear stress is increased to 1.7:1, as in the 30° samples, a larger effect is seen. In the high rate test shown in Figure 24, larger events are detected only in the last six seconds of loading (about 1 MPa) and again only accounts for a small portion of events detected. In the low rate test, however, the average event energy begins to steadily increase about six minutes prior to failure (at approximately 103 MPa). These events account for approximately 40% of those detected.

RAMP/HOLD EXPERIMENT

Results from the ramp/hold experiment, as shown in Figure 25, indicate that the average arrested crack length of microcracking in 90° samples also stays consistent during hold periods. There is apparently no loading rate effect. With the exception, perhaps, of the second ramp, there is no trend in the average event energy during each period.

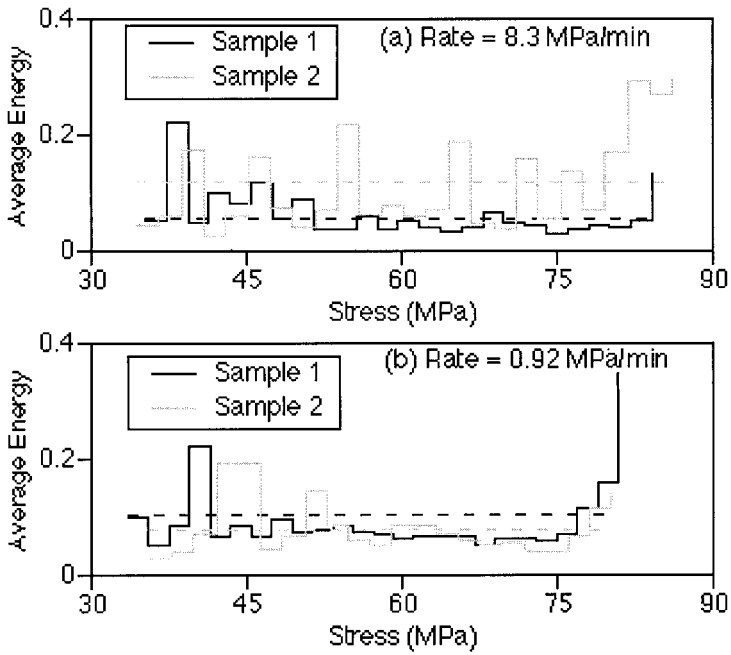


Figure 21. Average event energy detected in 45° off-axis samples at two load rates. The mean energy of all events is shown by the dotted line.

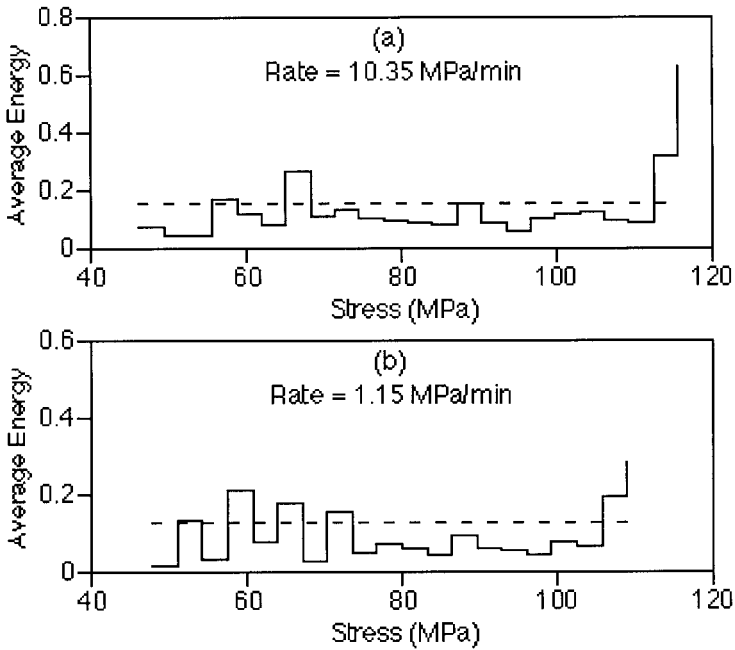


Figure 22. Average event energy detected in 30° off-axis samples for two loading rates. The mean energy of all events is shown by the dotted line.

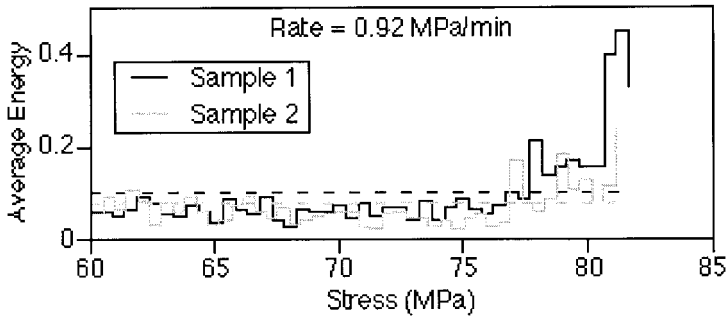


Figure 23. Average event energy detected in two 45° off-axis samples from 30 MPa to failure for two loading rates. The mean energy of all events is shown by the dotted line.

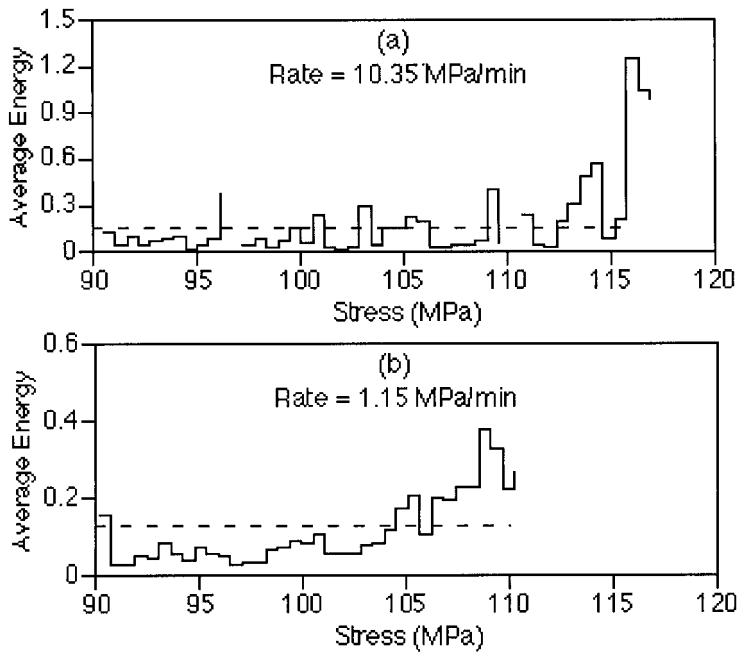


Figure 24. Average event energy detected in 30° off-axis samples from 90 MPa to failure. The mean energy of all events is shown by the dotted line.

Location of Large Events

The increase in average waveform energy discussed in the previous section may indicate a general increase in arrested crack length at high stress in the off-axis samples. However, these events may be occurring in an isolated region of the material, not uniformly distributed in the free length. To study the location of these larger cracks, waveforms detected before and after the increase in waveform energy were separated. Prior to the increase in energy, microcracking was uniformly distributed between the sensors as previously discussed.

The location of a subset of the events detected after the increase in waveform energy (those with maximum amplitude greater than 200 mV) were found as shown in Figure 26

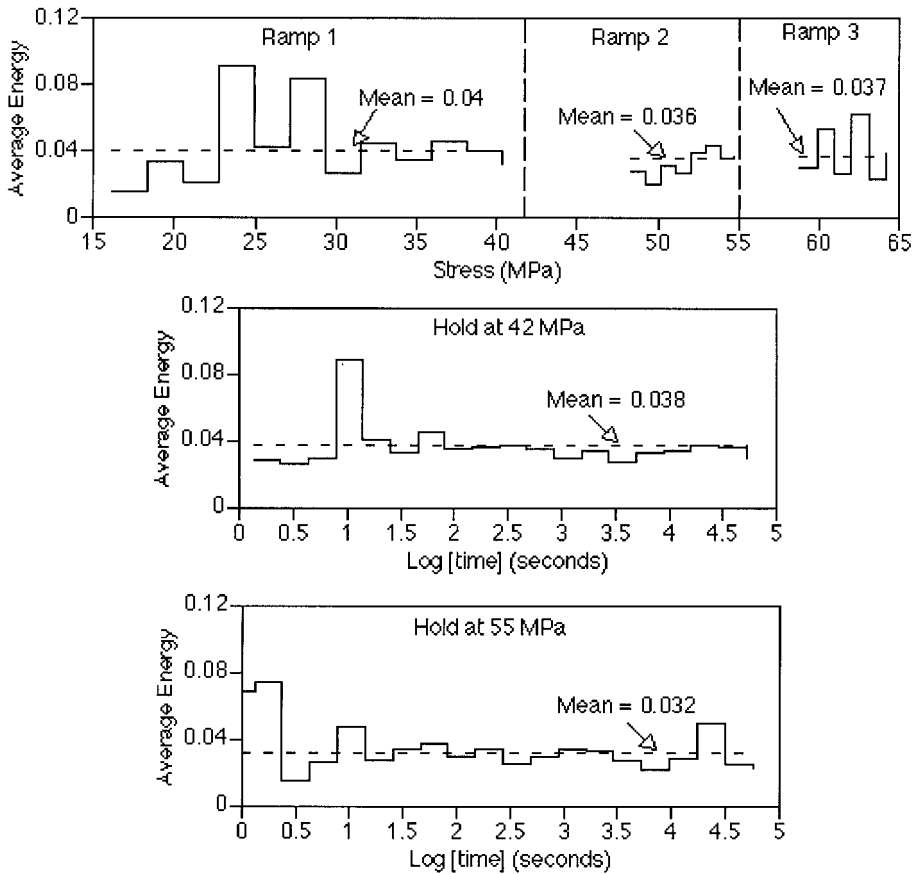


Figure 25. Average event energy during the ramp and hold periods of testing. Note that the ramp periods are vs. stress and the hold periods are vs. log(time). The mean energy of events for each period is shown by the dotted line.

for a 30° off-axis sample. Here there is a concentration of microcracking in a small region of the sample. A similar concentration occurred in the 45° off-axis samples. This concentration may indicate the beginning of crack interaction where a larger crack is created than would be otherwise. Global shear stress is not present in 90° samples to reorient and arrest such large cracks at the fibers, failure occurs instead. Thus this behavior is physically reasonable. It may also simply indicate a region of material that is relatively 'weaker' or less able to arrest crack growth under certain loading conditions. Regardless, this microcracking is not indicative of the distributed cracking and only occurs in the final stages of loading.

DATA ANALYSIS

Interpretation of AE Results

Unidirectional material in its as-manufactured state contains a distribution of small flaws or cracks that serve as initiation sites for microcrack growth. These are the voids,

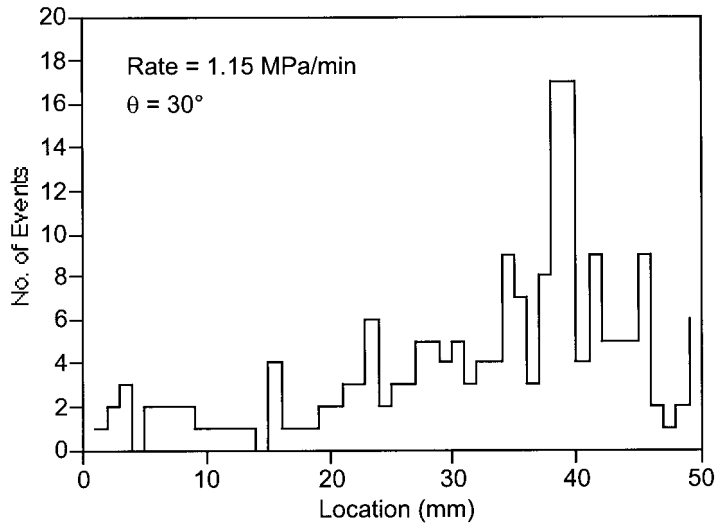


Figure 26. Location histogram of microcracking in the free length of a 30° off-axis sample. All events before the increase in average waveform energy have been removed and only events greater than 200 mV have been included. Note that this distribution was calculated assuming all cracking occurred along the centerline of the sample.

cracks around voids and fiber–matrix debonds that were viewed by Wood and Bradely [3] prior to loading the material. As the composite is loaded, some of these flaws become unstable, propagate at high speed, and arrest upon reaching a crack inhibitor (fiber, reduced stress zone, etc.). For example, Wood and Bradely [3] observed that the cracks around voids coalesced with debonded fibers around it. Each flaw has its own distinct initial crack geometry, local stress field (which depends on the microstructure in the vicinity of the crack tip) and fracture energy or process zone. Fiber–matrix debond is the same except there is an adhesive-type failure. As the material fails, energy is transferred from the continuum and to, among other things, an acoustic wave which is detected with the AE sensors.

If the material were elastic, each flaw would fail (become unstable) at a given level of globally applied stress. For a given volume of material, if we could count the number of cracks which fail at each level of global stress, a histogram of the number of cracks which initiate growth at each stress level could be found. This histogram would reflect the distribution of initial crack lengths and orientations, local stress concentrations (due to local geometry) and fracture energies of the initial flaws. This distribution should be common to all samples manufactured in a similar fashion. A major goal was to find this distribution of flaws.

It has been assumed that not all matrix-cracks are detected with the acoustic emission sensors. Some are arrested quickly, thus not emitting a strong acoustic wave. Others, depending on the loading, may not grow dynamically but instead exhibit slow sub-dynamic growth. However, only a statistically significant number needs to be detected to get an accurate measure of the distribution. Testing one coupon gives the same information as cutting small samples around each flaw and testing these individually to find its fracture stress and time.

Recognizing that not all matrix-cracks are detected with the acoustic emission sensors and that variations in the 'detectability' of events can change during a test, three items must be held constant to ensure that the correct distribution of flaws is found:

1. The volume of material over which microcracking is detected.
2. The minimum size of microcracks being detected.
3. The portion of microcracks detected.

If stress affects the arrested crack length, the portion of cracks detected throughout a test will change. However, as previously discussed in the section on waveform energy, this was not found to be the case, except in the lowest-rate 30° sample. Alternatively, to determine whether cracking becomes less detectable, the maximum amplitude may be used in this study. To maintain the same sampling of events in a material where arrested crack size is a function of stress level, the increase in average event amplitude may be used to account for this effect. By scaling the voltage threshold for which an event is accepted with the increase in average event amplitude, the same portion of cracks will be counted throughout the test.

Loading the material may also have an effect on both wavespeed and damping as the stiffness of the material changes as damage is introduced throughout the volume. If wavespeed drops, and we assume it to be constant throughout the test, the volume of material from which events are accepted will decrease and fewer events will be registered. If damping increases, the minimum size of detectable microcracks will grow throughout the test. A study of material acoustical properties was performed for these reasons.

Change in Material Acoustical Properties

To study the effect of material softening on the acoustical properties, microcracking waveforms were simulated using the AE-CAL equipment manufactured by Physical Acoustics Corporation. The same experimental setup as shown in Figure 17 was used for this study except one of the B225 sensors (previously used for location) is now used as a pulsing sensor. A 90 and 30° off-axis sample was ramped and held at various stress levels where the sensor was pulsed at 150 and 300 kHz.

Using Sensors 2 and 3 to differentiate extensional and flexural waveforms, the waves produced in both 90 and 30° off-axis samples were predominantly extensional as desired. Wavespeed of the extensional mode was measured from the arrival times at Sensors 2, 3 and 4. This speed was found to vary less than 5% in 90 and 30° off-axis samples from zero load to the highest stress tested. However, there was an effect on damping.

The maximum amplitudes of the extensional and flexural modes measured at Sensors 2 and 3 at various load levels are shown in Figures 27 and 28. From the stress level at which events are first detected, the maximum decrease in amplitude is at most 12% (300 kHz extensional mode in the 90° sample). One could correct for this effect by weighting the number of events detected by these ratios, but the changes are small enough that the measured distribution of flaws was not significantly affected, and no corrections were made. A better procedure would be to take a continuous measurement of wavespeed and amplitude during the entire loading period for all frequencies of interest. If there were significant changes, this information could be used to calibrate location calculations and event acceptance magnitude to maintain consistent sampling of the population of flaws.

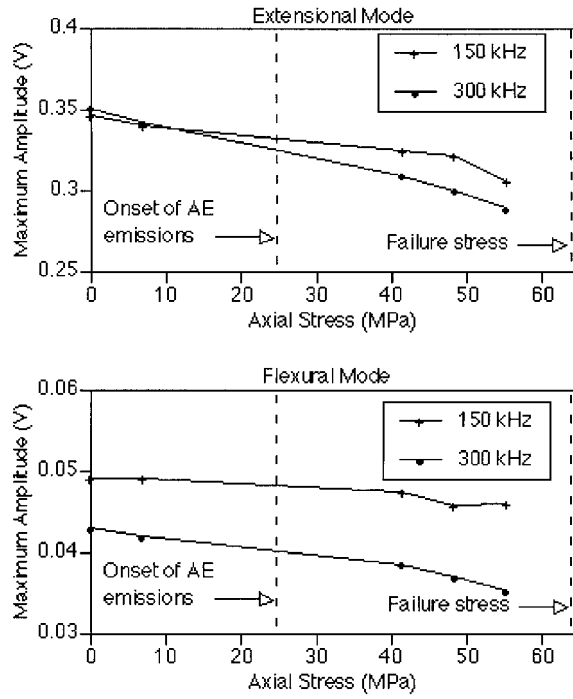


Figure 27. Maximum amplitude of the pulsed waveforms in a 90° sample at 150 and 300 kHz vs. axial stress.

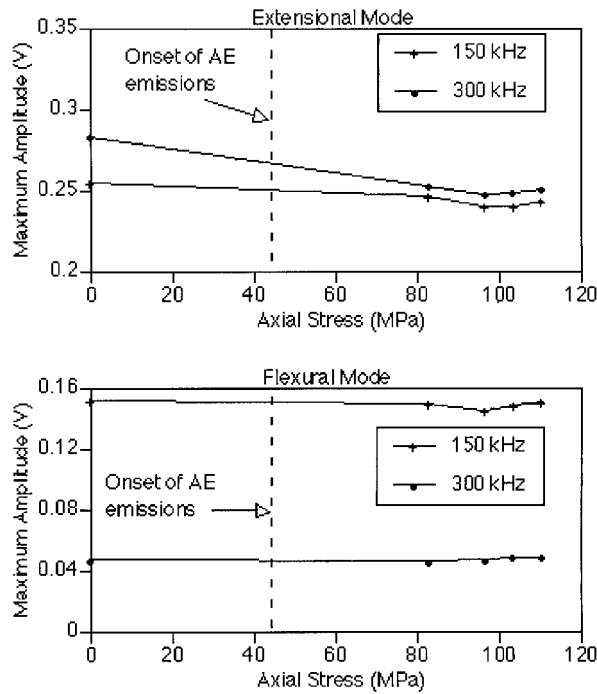


Figure 28. Maximum amplitude of the pulsed waves in a 30° sample at 150 and 300 kHz vs. axial stress.

Cumulative Distribution Function of Microcracking

The wide variation in cumulative event count from sample to sample may mask the rate-effects of microcracking. Sensor placement, coupling, choice of the region of material to be tested, thickness, variation in sensor sensitivity and many other factors can affect the total number of events detected. Regardless, these data can be used to construct a distribution function of the microcracking in the material. As already discussed, for an elastic material each flaw will fail at a given global stress value. The probability distribution function $p(\sigma)$ is defined by

$$p(\sigma)d\sigma = \frac{n_\sigma}{M}d\sigma \quad (3)$$

where $n_\sigma d\sigma$ is the number of flaws which grow dynamically between stresses σ and $\sigma + d\sigma$, and M is the total number in the free length of the material. Given that a statistically significant number of these flaws are detected by the AE sensors, M and $n_\sigma d\sigma$ can be interpreted as the quantities detected and not the actual totals in the material. The cumulative distribution function (CDF) is therefore,

$$P(\sigma) = \int_0^\sigma p(\sigma) d\sigma \quad (4)$$

In physical terms, $P(\sigma)$ gives the fraction of flaws that have failed, or run dynamically, up to a given stress. That a statistically significant number of microcracks were detected is supported by the derived distributions being independent of the threshold used for accepting events. Having confirmed that the volume of material, portion of flaws and the minimum size of detectable flaws stays essentially constant throughout a test, a histogram of events versus axial stress was used to calculate the CDF of microcracking for all sample types and loadings.

The CDF of microcracking detected in 90° samples is shown in Figure 29 for all ramp loadings where each curve represents the average of multiple samples (2 to 3). Similar

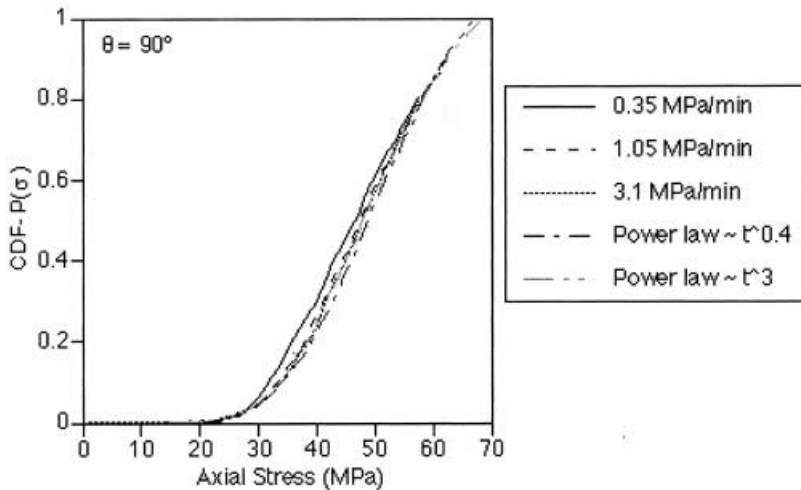


Figure 29. Cumulative distribution function of AE events detected from 90° samples loaded with different histories when using axial stress as the distribution parameter.

distributions were found for all monotone increasing loadings indicating that time or rate-dependence of the microcracking in 90° samples was very weak. The rate effect is only evident from ramp/hold and load/unload testing as shown in Figure 30. With the addition of shear stress, as in the off-axis samples, the rate effect on cracking becomes much stronger, as shown in Figure 31. Clearly, the microcracking does not depend on stress level alone. Analysis of the rate-dependent microcracking is beyond the scope of this paper and can be found in ([24,30,31]). In this work, a single distribution parameter is found, accounting for both load history and fiber angle, that results in a single CDF from all

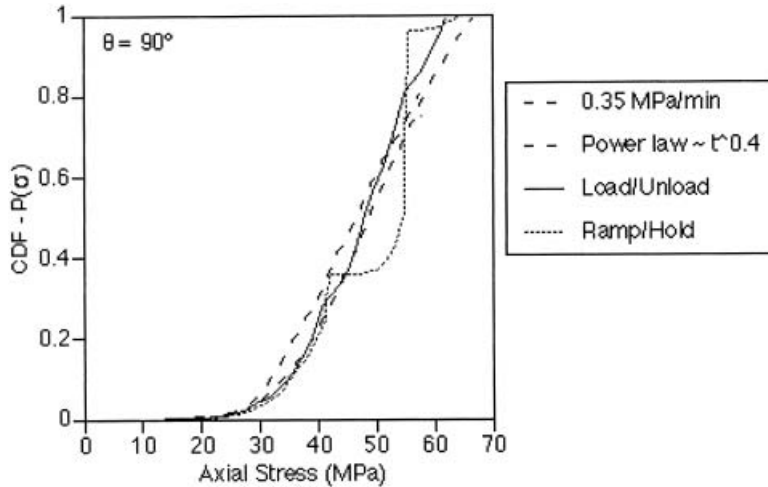


Figure 30. Cumulative distribution function of AE events detected from 90° samples using axial stress as the distribution parameter. Results from the load/unload testing and ramp/hold testing are compared with the other loadings.

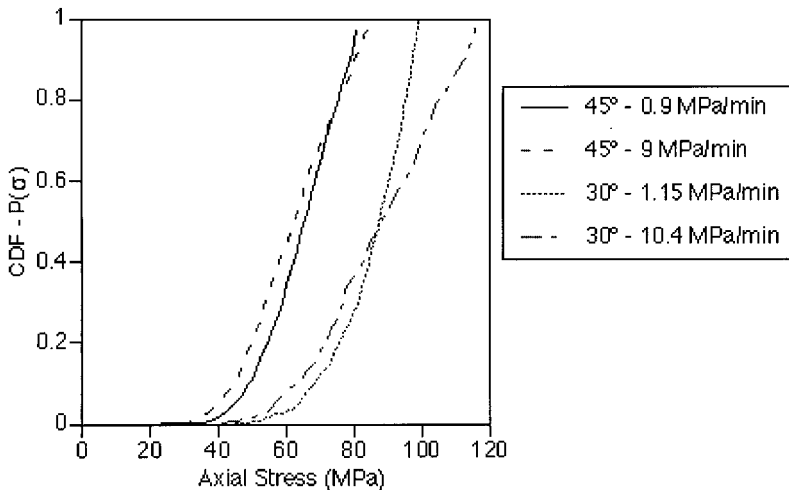


Figure 31. Cumulative distribution function of AE events detected from off-axis samples loaded with different rates when axial stress is used as the distribution parameter. No adjustments to the 30° data at 1.15 MPa/min have been made to account for the increase in waveform energy detected.

sample types. The issue of dynamic and subdynamic crack growth, and its effect on the derived distributions is discussed in [31].

CONCLUSION

Significant microcracking, evenly distributed along the free-length of all sample types, was detected with the AE sensors during loading. This microcracking, detected from the uniformly stressed portion of the material, accounted for only a small portion of the events acquired. After removing acoustic events from other sources, it was found that the onset of nonlinearity in the stress–strain response of 90° samples coincided with the onset of microcracking. No microcracking was detected by the AE method in room temperature tests of two untoughened composites that did not display nonlinear stress–strain behavior.

Distributed microcracking in the material emitted a variety of acoustic waves depending on the size of the crack and the local fracture energy of the material that failed. However, a histogram of waveform energy with stress-level showed that average waveform energy was constant from first microcracking to failure, except just prior to failure in off-axis samples. In these samples, the larger waveforms were isolated to a specific region of material and not indicative of the distributed cracking. It is believed that this implies the average arrested crack length is not a function of stress level. Microcracks that initiate at low stress propagate the same average distance as those that initiate at high stress. It seems physically reasonable that in this fiber composite arrested crack length is dictated by the fiber-related microstructural geometry and not by the loading history.

Use of a four-sensor setup, with two adjacent sensors and two location-sensors, was successful in differentiating the extensional and flexural waveforms detected from 90 and 30° off-axis samples. This method allows a direct comparison of waveforms between sample types as the waveforms have not been attenuated differently. Relative magnitude of the plate modes, waveform shape, frequency content and signal duration were all found to be similar in the waveforms acquired from 90 and 30° off-axis samples. Based on these observations, there is no evidence of a significant difference in the type of microcracking in the 90° and off-axis samples.

Each acoustic event originating in the ‘free-length’ of a sample was interpreted as the dynamic growth of an initial flaw or crack, resulting in a larger matrix crack or fiber–matrix debond. Many variables, including sensor choice, sensor placement, coupling, choice of the region of material to be tested, thickness, and variation in sensor sensitivity affected the total number of microcracks detected and resulted in significant variation in cumulative event count from sample to sample. There was no apparent relationship between event count and the extent of material softening. Using a histogram of the number of microcracks detected at each stress level, a cumulative distribution function (CDF) of microcracking was constructed. In physical terms, this distribution function is the fraction of flaws that have failed (grown dynamically) up to a given stress level. Changes in wavespeed, damping and arrested microcrack length as the material is loaded were considered when constructing the CDF. This distribution was found to be identical when comparing samples loaded identically and more clearly showed the rate effect on microcracking than AE event counts. Time or rate-dependent microcracking in 90° samples was weak and only apparent in ramp/hold and load/unload experiments. With addition of the shear stress in the off-axis samples, the effect was much stronger. These distributions were independent of the threshold used for accepting events and, for the 90°

samples, independent of sensor-type. Thus, use of the CDF of microcracking appears to be more effective for comparing microstructural damage in different material systems than nonnormalized events where the ‘detectability’ of events may vary between materials due to differences in acoustical properties.

ACKNOWLEDGMENT

This research was sponsored by the National Science Foundation and Mineral Management Services through The Offshore Technology Research Center.

REFERENCES

1. Nairn, J.A. and Hu, S. (1994). *Damage Mechanics of Composite Materials*, Elsevier, London.
2. Moore, R.H. and Dillard, D.A. (1990). *Composites Science and Technology*, **39**: 1–12.
3. Wood, C. and Bradely, W.L. (1997). *Composites Science and Technology*, **57**: 1033–1043.
4. Kamimura, K. (1985). *Mechanical Characterisation of Load Bearing Fibre Composite Laminates*, Elsevier, London.
5. Talreja, R. (1985). *Proc. Roy. Soc. London*, **399**: 195–216.
6. Schapery, R.A. (1987). *Polymer Engineering and Science*, **27**: 63–76.
7. Schapery, R.A. (1990). *J. Mech. Phys. Solids*, **38**: 215–253.
8. Schapery, R.A. (1989). In: Reddy, J.N. and Teply, J.L. (eds.), *Mech. Comp. Mat. and Structures*, ASME AMD Vol. 100, pp. 1–9.
9. Schapery, R.A. and Sicking, D.L. (1995). In: Bakker, A. (Ed.), *Mechanical Behaviour of Materials*, pp. 45–76, Delft University Press, Delft, The Netherlands.
10. Gustafson, C.G. and Selden, R.B. (1985). *Delamination and Debonding of Materials*, ASTM STP 876, American Society for Testing and Materials, Philadelphia.
11. Roy, C., Maslouhi, A. and Gaucher, D. (1988). *Canadian Aeronautics and Space Journal*, **34**: 224–232.
12. Wevers, M., Verpoest, I., De Meester, P. and Aernoudt, E. (1991). *Acoustic Emission: Current Practice and Future Directions*, ASTM STP 1077, American Society for Testing and Materials, Philadelphia.
13. Zimcik, D.G., Proulx, D. and Roy, C. (1988). *SAMPE Quarterly*, **19**: 5–11.
14. Chen, F., Hiltner, A. and Baer, E. (1992). *J. Composite Materials*, **26**: 2289–2307.
15. Komai, K., Minoshima, K. and Shibutani, T. (1991). *JSME International Journal*, **34**: 381–388.
16. Valentin, D. (1985). *Composites*, **16**: 225–230.
17. Wevers, M., Verpoest, I., Aernoudt, E. and De Meester, P. (1985). Mechanical Characterisation of Load Bearing Fibre Composite Laminates. In: *Proceedings of the European Mechanics Colloquium 182*, Elsevier, London.
18. Laroche, D. and Bunsell, A.R. (1980). International Conf. on Composite Materials (3rd), Balkema, Paris.
19. De Groot, P.J., Wijnen, P.A.M. and Janssen, R.B.F. (1995). *Comp. Sci. and Tech.*, **55**: 405–412.
20. Okoroafor, E.U., Huddleston, P.R. and Hill, R. (1996). *J. Materials Science*, **31**: 3057–3064.
21. Bocchieri, R.T. (1996). M.S. Thesis, The University of Texas at Austin.
22. Gorman, M.R. and Ziola, S.M. (1991). *Ultrasonics*, **29**: 245–251.
23. Prosser, W.H., Jackson, K.E., Kellas, S., Smith, B.T., McKeon, J. and Freidmant, A. (September 1995). *Materials Evaluation*, 1052–1058.
24. Bocchieri, R.T. (2001). PhD Dissertation, Department of Aerospace Engineering and Engineering Mechanics, The University of Texas at Austin.

25. Awerbuch, J., Gorman, M.R. and Madhukar, M. (1985). *Materials Evaluation*, **43**: 754–764.
26. CARP (1993). *J. Acoustic Emission*, **11**: 1–c24.
27. Daniel, I.M. and Ishai, O. (1994). *Engineering Mechanics of Composite Materials*, Oxford University Press, New York.
28. Sun, C.T. and Berreth, S.P. (1988). *J. Composite Materials*, **22**: 766–779.
29. Bocchieri, R.T. and Schapery, R.A. (2000). *Time Dependent and Nonlinear Effects in Polymers and Composites*, *ASTM STP 1357*, pp. 238–265, American Society for Testing and Materials, Philadelphia.
30. Bocchieri, R.T. and Schapery, R.A. (2002). Submitted to *Mechanics of Time-Dependent Materials*.
31. Bocchieri, R.T. and Schapery, R.A. (2002). Submitted to *Int. J. Fracture*.